Delft University of Technology

Benchmarking FeCr empirical potentials against density functional theory data

Klaver, TPC; Bonny, G; Olsson, P; Terentyev, D

Important note
To cite this publication, please use the final published version (if applicable).
Please check the document version above.

Benchmarking FeCr empirical potentials against Density Functional Theory data

T. P. C. Klaver[1], G. Bonny[2], P. Olsson[3], D. Terentyev[2]

[1]Department of Materials Science and Engineering, Delft University of Technology, Mekelweg 2, 2628 CD Delft, the Netherlands, t.p.c.klaver@qub.ac.uk
[2]SCK-CEN, Nuclear Materials Science Institute, Boeretang 200, B-2400, Mol, Belgium
[3]Department of Materials and Mechanics of Components, EDF-R&D, Les Renardières, F-77250 Moret-sur-Loing, France

Abstract

Three semi-empirical force field FeCr potentials, two within the formalism of the Two Band model and one within the formalism of the Concentration Dependent model, have been benchmarked against a wide variety of Density Functional Theory structures. The benchmarking allows an assessment of how reliable empirical potential results are in different areas relevant to radiation damage modeling. The Density Functional Theory data consists of defect-free structures, structures with single interstitials and structures with small di- and tri-interstitial clusters. All three potentials reproduce the general trend of the heat of formation quite well. The most important shortcomings of the original Two Band model potential are the low or even negative heat of formation for Cr-rich structures and the lack of a strong repulsion when moving two solute Cr atoms from being second-nearest neighbours to nearest neighbours. The newer Two Band model potential partly solves the first problem. The most important shortcoming in the Concentration Dependent model potential is the magnitude of the Cr-Cr repulsion, being too strong at short distances and mostly absent at longer distances. Both Two Band model potentials do reproduce long range Cr-Cr repulsion. For interstitials the Two Band model potentials reproduce a number of Cr-interstitial binding energies surprisingly well, in contrast to the Concentration Dependent model potential. For Cr interacting with clusters, the result can sometimes be directly extrapolated from Cr interacting with single interstitials, both according to Density Functional Theory and the three empirical potentials.

1 Introduction

Atomistic modeling of FeCr alloys has been a very active area of research during the last decade, see [1-3] and references cited therein. Much of the interest in FeCr has been driven by the promising properties of bcc FeCr alloys for nuclear applications [4, 5], i.e. a high resistance to radiation swelling compared to austenitic Fe-Cr-Ni alloys, a relatively high ductile-to-brittle transition temperature and low-activation properties. Apart from application in nuclear environments it is also an interesting alloy from a scientific point of view. The heat of formation (h.o.f.) is slightly negative for Fe-rich concentrations but then, rather unusually, changes sign to become strongly positive for equimolar and Cr-rich concentrations [6-9]. This behaviour is reflected in the experimentally observed short range order [10, 11] and unusually large solubility of Cr [12] at low Cr concentrations (< 10 at.% Cr). Also of scientific interest are the presence in the phase diagram of the complex σ phase [13] and the mixing of ferromagnetic Fe with anti-ferromagnetic Cr which leads to various interesting magnetic effects that influence the solubility of Cr in Fe [9].
The buildup of radiation damage is an inherently multiscale phenomenon. Computational studies of radiation damage often employ a multi-scale hierarchy of modeling methods, ranging from very accurate first principles calculations that can presently deal with hundreds of atoms at most, to physically very simple continuum models that can deal with calculations on a real-world scale. One method that in terms of accuracy lies in between these two opposite ends is the use of empirical force field potentials. A few years ago two empirical potentials for FeCr were developed, one by Caro *et al* in the Concentration Dependend model [14] (henceforth CDMpot) and one in the Two-Band model (using the PAW data) by Olsson *et al* [15, 16] (henceforth 2BMpot). At the time of their development, quite a few of the insights that were later revealed by Density Functional Theory (DFT) were still unknown. Thus much of the complexity was not taken into account while constructing the potentials. One could therefore be forgiven for being pessimistic about the chances that these potentials have to accurately reproduce what is now know about FeCr. Apart

from potential shortcomings due to unknown data, the 2BMpot was constructed with a symmetrical h.o.f., i.e. not only is there a slightly negative h.o.f. for some Fe-rich structures, but also for some Cr-rich structures. The latter has not been observed in experiments or *ab-initio* calculations and is therefore considered a shortcoming in the 2BMpot.

In this paper we will present the results of benchmarking of the two potentials mentioned above, as well as for a recently fitted Two-Band model potential by Bonny *et al* (henceforth Bon2BMpot) that addresses the problem of the negative h.o.f. for Cr-rich structures. A large number of configurations that were previously calculated with DFT have been re-calculated with the empirical potentials. Section 2 gives details about the DFT calculations and the empirical potentials and describes what configurations were calculated. Section 3 briefly describes some DFT results of Cr-interstitial cluster interaction that had so far not been reported. Section 4 lists the benchmarking results that show the strengths and weaknesses of the three potentials for different kinds of data. Conclusions are given in section 5.

2 Computational details

The DFT data that was used for benchmarking covers defect-free configurations, configurations with a single interstitial and configurations with di- and tri-interstitials. The defect-free configurations are the basis of the results reported in [9]. Most of the configurations in that paper plus a few others were re-calculated with the potentials. As with the defect-free DFT calculations, supercells up to 3x3x3 bcc cells were fully relaxed at zero pressure. Full details of the DFT calculations are given in [9].

The single interstitial configurations are the basis of the results presented in [17]. Systems containing a single interstitial in the middle of a 4x4x4 bcc cell supercell were relaxed at the fixed equilibrium volume of Fe. The interstitials had one or two Cr atoms inside the dumbbell as well as up to four Cr atoms on lattice positions nearest-neighbour to the dumbbell centre. Apart from the Cr inside or near the dumbbell, many supercells had 12 single solute Cr atoms positioned on the side faces of the supercells. These solute atoms were placed on the side faces to put as much distance between them and the dumbbells as possible. These latter Cr atoms will be referred to as 'background Cr' from now on. Full details about the DFT settings and the systems calculated are given in [17].

The calculations of Cr interacting with di- and tri-interstitials were carried out in 5x5x5 bcc supercells. As for the single interstitial DFT calculations, we used the PAW method [18, 19] implemented in VASP [20, 21]. Most of the settings used were the same as for the single interstitial DFT calculations, see [17]. A 3x3x3 k-point sampling proved sufficient for convergence of energy differences. The di- and tri-interstitials had one or two Cr atoms placed inside them or near them. The small interstitial clusters were calculated both in a background of pure Fe and in the presence of 24 monatomically dispersed background Cr atoms. The background Cr atoms were placed at a distance from the cluster centres similar to the distance between the background Cr and centres of the single interstitials. Figure 1 shows an example of a 4x4x4 supercell with a single interstitial and background Cr atoms and a 5x5x5 bcc cell supercell with a tri-interstitial and background Cr atoms. In all, more than 200 configurations without interstitials, single interstitials and small interstitial clusters were compared. While radiation damage also creates vacancies, we did not benchmark Cr-vacancy interaction, as it is not very strong in Fe-rich FeCr. Experiments [22] show for example that the onset temperature of stage III in resistivity recovery experiments is independent of Cr concentration. Atomistic simulations with all three empirical potentials also show that the interaction is not very strong at any distance. Hence a detailed benchmarking of Cr-vacancy interaction would produce numbers that are all rather close to 0, the question of how close exactly being less interesting.
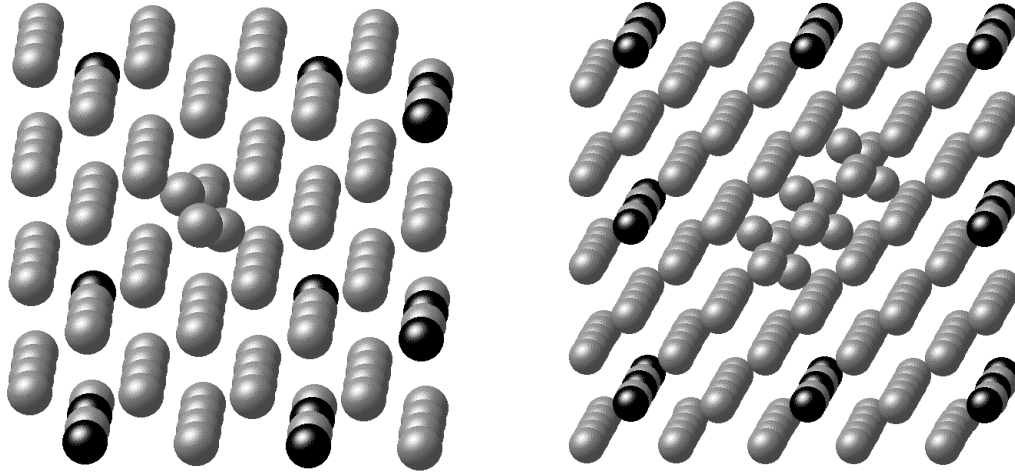
Figure 1. 4x4x4 and 5x5x5 bcc cell supercells with an interstitial or tri-interstitial at the centres and monatomically dispersed background Cr (black atoms) 'far away' from the centres.

The CDMpot was used as published by Caro *et al* [14]. It is an Embedded Atom Method (EAM) type potential. The embedding part of the potential if fairly small, most of the interaction comes from the pair potential. All the local concentration dependent behaviour comes from the pair potential, akin to the Redlich-Kister expansion [23] of the Calphad methodology [24]. The pair potential contains the mean of the pure element pair potentials of Fe and Cr, multiplied by a function that depends on concentration. The heat of formation, calculated over the entire concentration range by electronic structure methods, is the only fitting target for the CDMpot.

The 2BMpot, developed in the framework of the Tight Binding second-moment approximation, follows a different approach [15, 16]. Like the CDMpot, it is an EAM potential, but it accounts for contributions from s-band electrons by adding a second embedding term to the EAM energy, similar to the work of Ackland and Reed [25]. It is fitted to the FeCr lattice parameter of an $Fe_{90}Cr_{10}$ alloy, the positive heat of formation of an equimolar alloy, the substitution energy of a single Cr atom and the binding of solute Cr to the <110> dumbbell (all values fitted to the VASP DFT data set in [15]).

Though based on different physical grounds, both formalisms introduce terms dependent on local concentration and it can be shown that they are equally capable of reproducing concentration dependent bulk properties [26].

The Bon2BMpot is a variation to the 2BMpot that features different embedding functions for the s-electron density of Fe and Cr. This allows avoiding the low or even negative h.o.f. for Cr-rich structures. The Bon2BMpot was also fitted to different data that includes more Cr-rich structures than the data to which the 2BMpot was fitted.

To make a one-to-one comparison with the DFT data, the relaxed DFT configurations were re-relaxed with the empirical potentials, using the conjugate gradient method.

The cut-off range for the three potentials is 5.3 Å, with the interaction range in the EAM formalism being twice the cut-off range. With this interaction range and the size of our interstitial systems, the benchmarking will not only test the accuracy of short range Cr-Cr and Cr-interstitial interaction, but also test how well the potentials reproduce the important long-range Cr-Cr interaction (figure 1 in [27]).

The results in this paper come in terms of formation, binding and clustering energies. The formation energy E_f of a system of n atoms with composition Fe_xCr_{1-x} is calculated using

$$\Delta E_f = E(nFe_xCr_{1-x}) - xnE(Fe) - (1-x)nE(Cr) \tag{1}$$

where $E(nFe_xCr_{1-x})$ is the total energy of the system with n atoms and composition Fe_xCr_{1-x}, $E(Fe)$ and $E(Cr)$ are the energies per atom of Fe and Cr in their pure equilibrium states. The binding energy E_b between objects (e. g. the binding energy that is released when a solute Cr atom and a dumbbell self-

interstitial merge to become a mixed dumbbell) is defined as the formation energy difference between a system in which the objects are close together and a system in which all the objects are far apart. Within the limited size of our systems it is not possible to separate objects over large distances. Therefore the formation energy of the situation where the objects are separated is usually calculated by calculating each object individually in a supercell. The binding energy for merging n objects then becomes

$$E_b = -\left(E_f(combined) - E_f(object1) - E_f(object2) - \ldots\ldots\ldots - E_f(objectn)\right) \tag{2}$$

in which a positive binding energy means attraction between the objects, a negative binding energy means repulsion. When determining the binding energy of objects in the presence of background Cr, eqn. (2) should be used in a slightly modified form to prevent the formation energy of the background Cr from playing a part in the binding energy. The modification consists of adding *n-1* times the formation energy of the background Cr to the 'merged side' if n objects are merged. Figure 2 shows an example where two objects, an interstitial and a single solute Cr atom, are merged in the presence of background Cr.
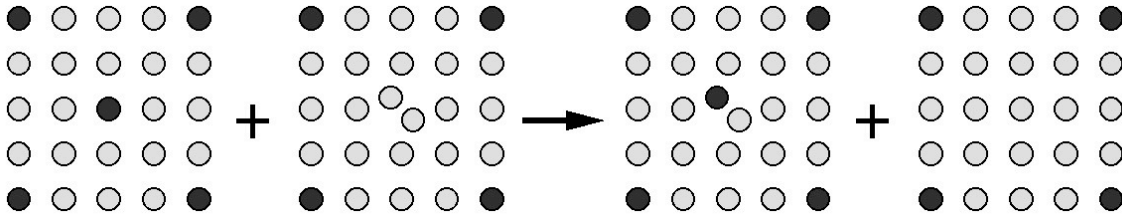

Figure 2. An example of determining the binding energy between objects in the presence of background Cr. Rather than determining the total formation energy difference between the two configurations on the left and the left-most configuration on the right, the formation energy of the background Cr is added on the right, so that the background Cr is accounted for the same number of times for the separate and merged situations.

Finally, the clustering energy is simply the energy change when going from a system with a number of monatomically dispersed solute Cr atoms at maximum possible distances from each other, to a system with similar numbers of Cr and Fe atoms, but with the Cr atoms clustered as nearest neighbours:

$$E_{cluster} = E_{clustered} - E_{dispersed} \tag{3}$$

3 DFT results of the interaction between Cr and di- and tri-interstitials.

We will now shortly list a number of DFT results about the interaction between Cr and small clusters of di- and tri-interstitials that had not been reported yet. One or two Cr atoms were placed in various positions inside or next to the small interstitial clusters. The di- and tri-interstitials were either regular clusters of nearest-neighbour parallel <110> dumbbells or non-parallel clusters that have formation energies close to the formation energies of regular clusters, see [28]. A non-parallel di-interstitial can take the form of three atoms sharing a single bcc lattice site, as first reported by Gao *et al* [29], three non-parallel <110> dumbbells can assume a low-energy configuration by forming an interstitial ring [28]. Clusters of similar configuration were embedded both in backgrounds of pure Fe and Fe dotted with monatomically dispersed background Cr atoms.

In many ways, the short-range interaction of Cr with small interstitial clusters is similar to the interaction between Cr and single <110> dumbbells. The binding energy between a Cr atom and the cluster, if any, is sometimes mere hundredths of eV and usually does not exceed 0.2 eV. For clusters of two or three parallel dumbbells or the ring-like tri-interstitial the weak binding is not surprising, as all these configurations consist of multiple <110> dumbbells and the binding of Cr to a single <110> dumbbell is usually weak [30-32] and could be somewhat stronger in concentrated alloys [33-35]. The interaction of one or two Cr atoms with a <110> dumbbell that is a part of a cluster is rather similar to the interaction with a single dumbbell, i.e. extra FeFe <110> dumbbells sitting next to an FeCr or CrCr dumbbell have little influence on the Cr-dumbbell binding. While less predictable, we observe that the mostly small interaction extends to Gao-type

'3-in-1' di-interstitials. For Gao-type di-interstitials the interaction is usually slightly repulsive. For both clusters consisting of dumbbells and Gao di-interstitials there are a few strongly repulsive configurations where it would be energetically favourable to keep the Cr atoms and interstitial clusters all separate. However, these configurations have multiple Cr atoms in them that are close together. The repulsion is therefore to a large extent due to Cr-Cr repulsion as in defect-free FeCr and in systems with a single interstitial, not due to Cr-cluster repulsion. Averaged over all Cr-clusters interactions in our data set, there is a small repulsion of some hundreths of eV between the Cr atom(s) and the clusters. Since short-range Cr-cluster interaction is mostly weak, the relative stabilities of parallel and non-parallel clusters does not change much due to the presence of nearby Cr.

The long-range interaction between monatomically dispersed background Cr and small clusters with Cr inside or near them is also in many ways similar to the interaction between background Cr and single interstitials with Cr. As in single interstitial systems, it extends to a considerable range. For all 38 configurations that were calculated both with and without background Cr, there was a repulsion between the background Cr and the cluster with Cr inside or near it. The average repulsion is 0.6 eV for the distance at which the background Cr atoms are placed from the clusters. The repulsion is easy to understand. The background Cr alone raises the Cr concentration to 9.6%. This is already more than the concentration where the FeCr heat of formation has its minimum, around 7-8% [9]. Adding a cluster with one or two Cr atoms to the system raises the Cr concentration, thereby moving the systems up to higher values on the heat of formation curve. The long-range repulsion is not significantly different for systems with parallel or non-parallel clusters. Since the short-range Cr-cluster interaction also did not favour one type over the other, we conclude that Cr alloying does not on average change the relative formation energies of parallel and non-parallel clusters compared to pure Fe.

Finally, one trend reported for Cr interacting with single dumbbells does not extend to Cr interacting with small clusters. Previously it was reported that the presence of background Cr enhances the binding between other Cr atoms and single interstitials. This conclusion was drawn on the basis of 4 configurations, two of which contained <110> dumbbells. However, for the 38 configurations in this study, no significant average increase in binding or reduced repulsion was observed. Cr-cluster binding energies in the presence of background Cr do differ from those in a pure Fe background by up to 0.2 eV, but there is no average bias toward binding or repulsion. We suspect that the previous conclusion about increased binding, based on a small number of single interstitial configurations, was probably down to coincidence.

4 Benchmarking results

4.1 Defect-free FeCr

The heat of formation (h.o.f.) of FeCr alloys shows the well-known small negative h.o.f. down to ~10 meV/atom [9, 27, 36] for Fe-rich concentrations, with a change of sign occurring around 12% Cr and the h.o.f. reaching up to ~100 meV/atom [9] around equi-molar concentrations, see figure 3. Different data points for one concentration represent supercells with different (clustered or dispersed) Cr configurations.
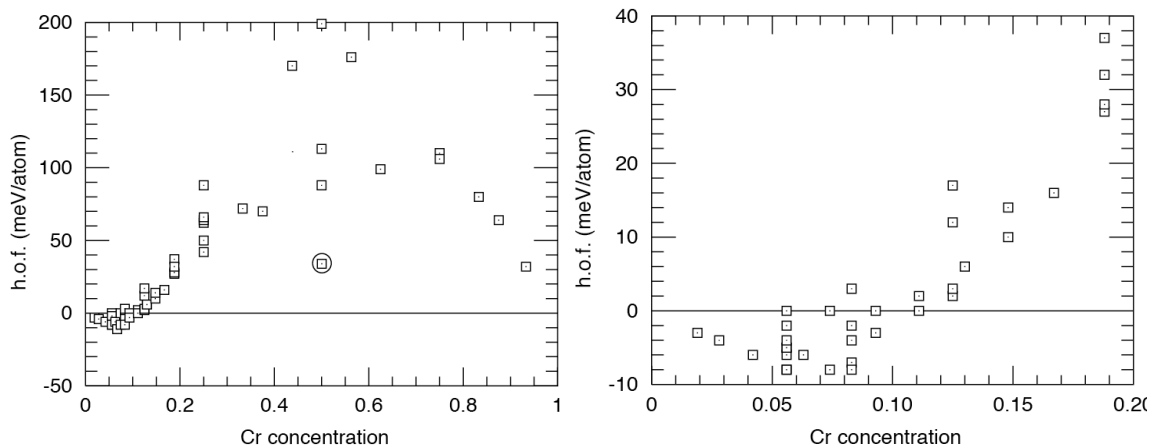
Figure 3. Left: the FeCr heat of formation, determined by DFT [9]. The data points with high formation energies (except the encircled data point) represent 'very mixed' system, i.e. Cr having mostly Fe neighbours and *vice versa*. Right: enlargement of the 0-20% concentration range.

Figure 4 shows the same data points as in figure 3 together with the data points for similar configurations re-relaxed with the empirical potentials.
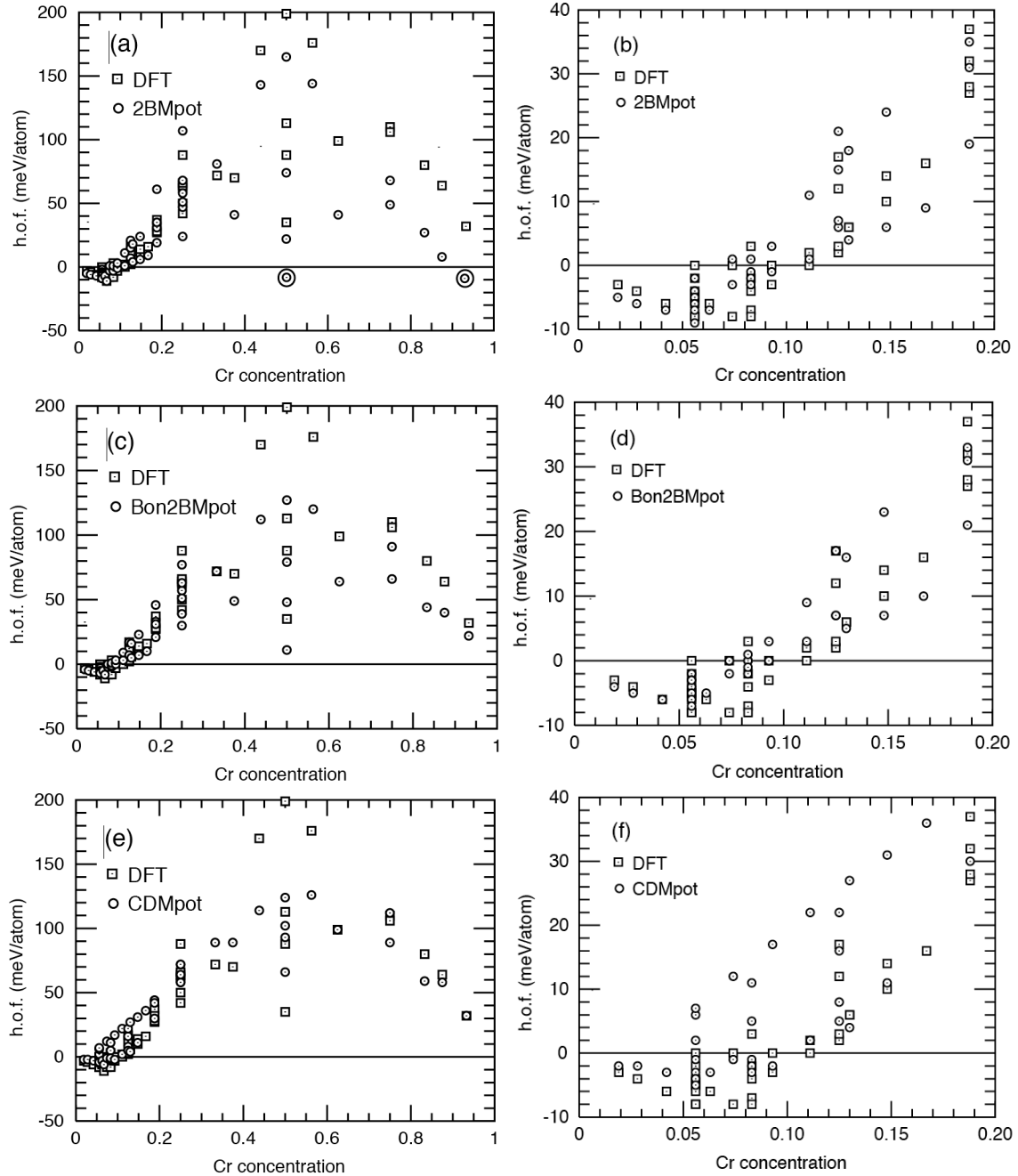

Figure 4. FeCr heat of formation (h.o.f.). The figures on the right show an enlargement of the ones on the left.

All three potentials manage to qualitatively reproduce the main features of the h.o.f. mentioned above and in the 0-10% Cr region they reproduce the lowest formation energies for the right structures (i.e. widely

dispersed Cr atoms). At higher Cr concentration, the 2BMpot generally gives formation energies that are too low, even giving negative values (encircled in figure 4A). While relaxation with the empirical potential significantly lowers the energy for some structures, even the unrelaxed energies of the DFT structures can already be too low or even negative. Ionic relaxations that are too strong are therefore not the most important factor underlying the formation energies that are too low or negative. The negative energies may lead to unphysical configurations resulting from simulations (e.g. Monte Carlo simulations) and form a serious drawback of the potential. The other two potentials do not suffer from the latter problem, although the Bon2BMpot potential still produces formation energies for Cr-rich structures that are too low. The formation energies of the Bon2BMpot in the Fe-rich end remain mostly unchanged compared to the 2BMpot. The CDMpot reproduces the general h.o.f. trend better than the 2BMpot and Bon2BMpot in that it does not suffer from the low h.o.f. for some structures around equimolar and Cr-rich concentrations. However the CDMpot has other problems. The negative h.o.f. for Fe-rich structures does not reach deep enough and the CDMpot also overestimates the energy required to bring Cr atoms together at low Cr concentrations. There is a line of data points for the CDMpot in figure 4f that rises linearly with Cr concentration and overestimates formation energies compared to the DFT data. These CDMpot data points correspond to clusters of 3-8 Cr atoms in 3x3x3 bcc cell supercells, see next.

In figure 5 the clustering energies obtained for different energy models are compared.
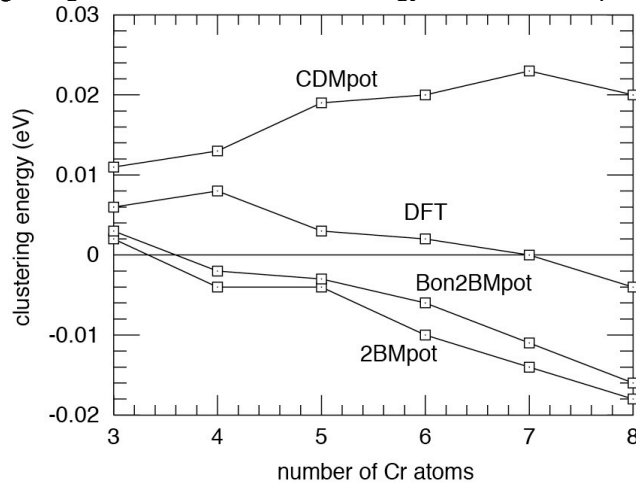

Figure 5. Comparison of clustering energies of 54 atom supercells with 3-8 Cr atoms calculated by DFT with the ones calculated by the three potentials.

All resulting curves show an essentially linear behaviour, with positive values indicating a tendency to ordering and negative values a tendency to clustering. Both 2BM potentials give a negative slope in close agreement with DFT, but are shifted down by about 10 meV. This suggests a stronger tendency towards Cr clustering than predicted by DFT. In contrast, the clustering energy for the CDMpot is positive for all reported cluster sizes and with a positive slope. Despite the poor agreement of the latter with DFT data, we note, however, that all potentials have been successfully applied in studies regarding Cr precipitation and short-range order [37-40].

The Cr-Cr repulsion resulting from DFT and the different potentials are compared in figure 6. From this figure we see that all three potential reproduce Cr-Cr repulsion suggested by the DFT data in the correct range. However, both 2BM potentials fail to reproduce the trend of decreasing interaction strength predicted by DFT below fourth nearest neighbour and also fail to produce the sharp decrease in energy when going from nearest to second-nearest neighbours. The CDMpot, on the other hand, while shifted overall, follows the trend of the DFT curve well.
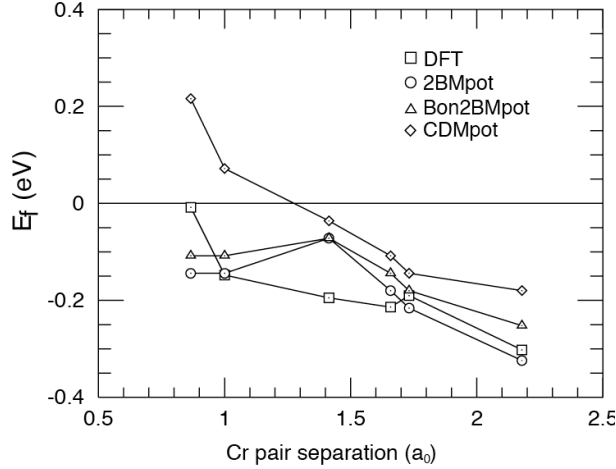
Figure 6. Formation energies of 3x3x2 bcc cell supercells, containing two solute Cr atoms at different separations, calculated with the three empirical potentials and DFT.

4.2 Cr interacting with single interstitials in Fe

In a number of cases the re-relaxation with the empirical potentials of the relaxed DFT structures resulted in a different relaxed interstitial configuration than the DFT configuration. This may be down to the parameters of the relaxation schemes in some cases, but in most cases it is because the configurations that are (local) energy minima in DFT are not minima according to the empirical potentials. In eight cases where the interstitial was placed in a local Cr enrichment the relaxation with DFT resulted in <221> dumbbell interstitials. The ground state for an interstitial in pure Cr is the <221> dumbbell [41] and in some cases six Cr atoms in Fe inside or near the dumbbell are enough to make the interstitial assume the <221> configuration. Unsurprisingly, none of the empirical potentials potential reproduced any of the <221> interstitials, mostly relaxing into <110> dumbbells instead. However, the 2BMpot does predict the interstitial ground state in pure Cr to be the <221> configuration. The <100> dumbbell was also found to be unstable according to all three empirical potentials (unless the relaxation was started from a perfectly symmetrical saddle point configuration), usually transforming into <100> crowdions. In addition to this, a few <111> and <110> dumbbells erroneously transformed into the other orientation with the 2BMpot. For systems where empirical potential relaxation did not result in a transformation a direct comparison between the system energies is possible.

The interaction between an interstitial and nearby Cr atom(s) is reproduced correctly in terms of sign and absolute value by both 2BM potentials (see table I and figure 7), as compared to DFT. The only configurations for which the sign of the interaction was not reproduced are the <111> Cr-Cr crowdion and for the 2BMpot also the CrCr <100> dumbbell. In contrast to that, the CDMpot fails to reproduce the correct sign of interaction for half of the cases and gives an interaction energy that is too repulsive for most of the configurations. The worst predictions with the CDMpot are found for CrCr interstitial configurations.

Table I. Formation energies E_f of solute Cr and interstitials in 4x4x4 bcc cell supercells, calculated with DFT and empirical potentials. In supercells with Cr and interstitials, the binding energies E_b between the Cr atom(s) and the interstitials is also reported. The configuration FeCr <110> + n.n. Cr is a mixed <110> dumbbell with a solute Cr positioned in the compressive lattice site next to the Cr inside the dumbbell.

Configuration	E_f, DFT E_b, DFT (eV)	E_f, 2BMpot E_b, 2BMpot (eV)	E_f, Bon2BMpot E_b, Bon2BMpot (eV)	E_f, CDMpot E_b, CDMpot (eV)
solute Cr atom in Fe	-0.11 -	-0.29 -	-0.24 -	-0.11 -
FeFe <110>	4.02 -	3.59 -	3.58 -	3.59 -
FeCr <110>	3.83	3.16	3.24	4.06

	0.08	0.14	0.10	-0.58
CrCr <110>	4.23	3.38	3.29	4.88
	-0.43	-0.37	-0.19	-1.51
FeCr <110> + n.n. Cr	4.01	3.22	3.26	4.59
	-0.21	-0.21	-0.16	-1.22
FeFe <111>	4.72	4.08	4.08	4.08
	-	-	-	-
FeCr <111>	4.24	3.40	3.53	4.02
	0.37	0.39	0.31	-0.05
CrCr <111>	4.28	3.59	3.51	5.39
	0.22	-0.09	-0.09	-1.53
FeFe <100>	5.13	4.39	4.38	4.39
	-	-	-	-
FeCr <100>	4.93	3.35	3.67	4.10
	0.09	0.75	0.47	0.18
CrCr <100>	5.28	3.68	3.98	5.94
	-0.37	0.13	-0.08	-1.77

Then, DFT calculations reveal that the relative stability of <110> dumbbells to <111> dumbbells decreases monotonously from FeFe to CrCr configuration (0.7 – 0.05 eV), as presented in Table II. Both 2BM potentials succeed to reproduce this trend, while the CDMpot predicts the same stability for FeFe and CrCr dumbbells. The FeCr <111> dumbbell was found to be the most stable configuration with the CDMpot, in contradiction to DFT data. With respect to the stability of <100> dumbbells to <111> dumbbells, DFT data show the opposite trend, i.e. replacing Fe atoms inside the dumbbell by Cr increases the relative stability of the <111> configuration. For the <100> <110> energy difference is mostly independent of the dumbbell occupation in DFT. All three potentials fail to reproduce the DFT trends involving <100> dumbbells.

Table II. Formation energy differences between dumbbells with different orientations for different chemical occupations.

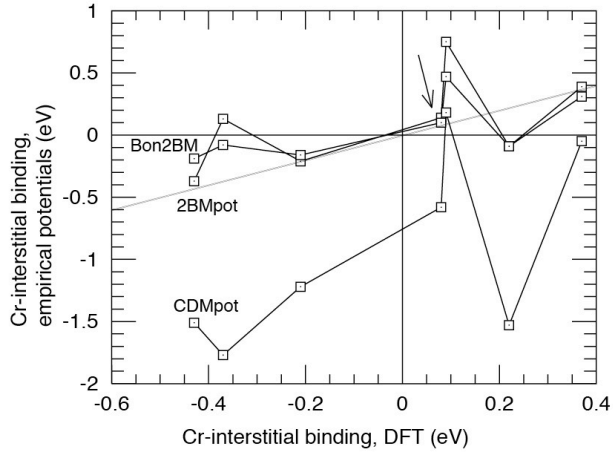| E_f<111>- E_f<110> (eV)				
dumbbell occupation	DFT	2BMpot	Bon2BM	CDMpot
FeFe	0.70	0.49	0.50	0.49
FeCr	0.41	0.24	0.29	-0.04
CrCr	0.05	0.21	0.22	0.51
E_f<100>- E_f<110> (eV)				
dumbbell occupation	DFT	2BMpot	Bon2BM	CDMpot
FeFe	1.11	0.80	0.80	0.80
FeCr	1.10	0.19	0.43	0.04
CrCr	1.05	0.30	0.69	1.06
E_f<100>- E_f<111> (eV)				
Dumbbell occupation	DFT	2BMpot	Bon2BM	CDMpot
FeFe	0.41	0.31	0.30	0.31
FeCr	0.69	-0.05	0.14	0.08
CrCr	1.00	0.09	0.47	0.55

Figure 7. Cr-interstitial binding according to empirical potentials against Cr-interstitial binding DFT data. The DFT binding energy of the data point marked with an arrow was included in fitting of the 2BMpot and Bon2BMpot. It should be noted that when the interstitial interacts with two Cr atoms, the binding energy also includes the repulsion from bringing two Cr atoms close together.

Finally, the repulsive interaction between a Cr background and a FeCr dumbbell, found in DFT calculations (see figure 8) is well reproduced by both Two-Band model potentials. In most of the inspected cases, the CDMpot shows weak attractive interaction, thus contradicting the DFT data. At the same time, the resulting interaction energy between an interstitial and nearby Cr atoms is on average not significantly influenced by the presence of the Cr background, as is found using all three potentials and confirmed by DFT.
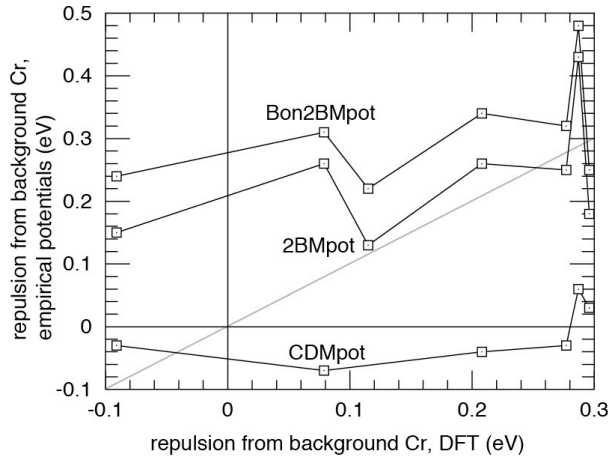

Figure 8. Repulsion from background Cr that is experienced by the interstitials with Cr inside or near them at the supercell centres. The values determined by the empirical potentials are shown against the data calculated with DFT. The repulsion was determined by calculating supercell formation energies with both the background Cr and interstitials with Cr present, only the background Cr, and only the interstitials with Cr inside or nearby. The repulsion is the formation energy of the supercell with both background Cr and interstitial with Cr atoms present minus the formation energies of just the background Cr and just the interstitial with Cr atoms.

4.3 Cr interacting with di- and tri-interstitials in Fe

Most of the di- and tri-interstitials relaxed with DFT also proved to be (local) energy minima with all three empirical potentials. None of the di- or tri-interstitials consisting of parallel dumbbells transformed and neither did any of the 3-in-1 'Gao' di-interstitials. However, re-relaxation of the 'ring' tri-interstitial lead to transformation in quite a few cases. Sixteen ring configurations with one or two Cr atoms inside or near them were relaxed, both in backgrounds of pure Fe and monatomically dispersed Cr. Re-relaxation with the

CDMpot lead to transformation in four cases out of 32. For both the 2BMpot and Bon2BMpot 17 configurations (not all the same ones) transformed.

Looking only at the structures that did not transform during re-relaxation, the results for the empirical potentials for clusters are in many ways similar to those for single interstitials. This was also found with DFT. As with DFT, the interaction between one or two Cr atoms and a <110> dumbbell is somewhat independent of the nearby presence of FeFe <100> dumbbells. Table III gives two examples.

Table III. Binding of one or two Cr atoms to a single <110> dumbbell and binding of one or two Cr atoms to a <110> dumbbell that is part of a parallel di-interstitial.

	E_b(Cr to single <110> interstitial dumbbell) (eV)	E_b(Cr to di-interstitial <110> dumbbell) (eV)
DFT	0.08	0.02
2BMpot	0.14	0.12
Bon2BMpot	0.10	0.03
CDMpot	-0.58	-0.51
	E_b(CrCr to single <110> interstitial dumbbell) (eV)	E_b(CrCr to di-interstitial <110> dumbbell) (eV)
DFT	-0.43	-0.48
2BMpot	-0.37	-0.40
Bon2BMpot	-0.19	-0.33
CDMpot	-1.51	-1.43

For DFT the extrapolation from single interstitial binding to small clusters is true for dumbbells that form both parallel clusters and ring-type tri-interstitials. For the empirical potentials the latter could not be checked, as most relevant ring-like structures transformed for the 2BMpot and Bon2BMpot. For Gao di-interstitials the 2BMpot and Bon2BMpot predict binding for half of the configurations calculated, while in DFT only one out of eleven configurations showed binding. While the 2BMpot and Bon2BMpot predict too many binding configurations, the magnitude of the binding is of the right order of magnitude, never bigger than 0.21 eV (the maximum binding in DFT being 0.15 eV). The CDMpot predicts unrealistically strong repulsion between Cr atoms and Gao di-interstitials, again mostly in cases of two nearby Cr atoms inside or near the di-interstitial.

For none of the three empirical potentials does the presence of background Cr significantly change the average binding between Cr and most di- and tri-interstitials, in agreement with DFT results. For the 2BMpot and Bon2BMpot the average overall binding and repulsion between Cr atoms and the clusters for all 38 cluster configurations calculated, both with pure Fe and dispersed Cr backgrounds, is just a few hundreths of eV for both backgrounds. This is in agreement with DFT results. For the CDMpot, there is an average repulsion of 0.5 eV for both backgrounds. As with single interstitials this is mainly due to the overly strong CrCr repulsion that makes it too difficult to bring multiple Cr atoms together inside or near an interstitial.

Finally, results for the long-range repulsion between background Cr and interstitial clusters with Cr inside or near them are also similar to the results for single interstitials. In DFT the average repulsion is 0.6 eV. The 2BMpot and Bon2BMpot give results that are of the right magnitude, i.e. 0.4 and 0.8 eV respectively. As with single interstitial configurations, the CDMpot results in a long-range repulsion that is far too weak at 0.07 eV on average.

Table IV summarizes the main results of benchmarking defect-free FeCr, single interstitial systems and configurations with interstitial clusters.

Table IV. Strengths and weaknesses of the three empirical potentials in reproducing DFT data.

benchmarked feature	2BMpot	Bon2BMpot	CDMpot

defect-free			
h.o.f.	good: - overall trend reproduced fairly well - both qualitative and quantitative reproduction of monatomically dispersed Fe-rich structures - ordering trend in Fe-rich region reproduced bad: - unphysical structures are stabilized at equimolar and Cr-rich concentrations	good: - overall trend reproduced well - both qualitative and quantitative good reproduction of monatomically dispersed Fe-rich structures - better agreement than 2BMpot with DFT for equimolar and Cr-rich structures, i.e., unphysical structures are no longer stabilized - ordering trend in Fe-rich region reproduced	good: - overall trend reproduced best of three potentials - ordering trend in Fe-rich region reproduced bad: - Cr solutes not stable enough
clustering in Fe-rich region	good: - qualitative agreement, i.e. Cr can cluster together bad: - poor quantitative agreement, too easy	good: - qualitative agreement, i.e., Cr can cluster together bad: - poor quantitative agreement, too easy	good: - qualitative agreement, i.e., Cr can cluster together bad: - poor quantitative agreement, too hard
repulsion between solute Cr atoms in Fe-rich region	good: - qualitative agreement, i.e., Cr-Cr pairs repel bad: - fails to reproduce a drop of the repulsive interaction between 1st and 2nd nn Cr-Cr pair configurations - spurious high energies at third-nearest neighbour distance - repulsion not strong enough	good: - qualitative agreement, i.e., Cr-Cr pairs repel bad: - fails to reproduce a drop of the repulsive interaction between 1st and 2nd nn Cr-Cr pair configurations - spurious high energies at third-nearest neighbour distance - repulsion not strong enough	good: - monotonic energy decline with distance reproduced - reproduces a drop of the repulsive interaction between 1st and 2nd nn Cr-Cr pair configurations
single interstitials			
stability	bad: - no stable <221> dumbbell in Cr enrichment - some other dumbbells also transformed	bad: - no stable <221> dumbbell in Cr enrichment - some other dumbbells also transformed	bad: - no stable <221> dumbbell in Cr enrichment - some other dumbbells also transformed
local Cr binding to interstitial	good: - some binding energies reproduced very accurately, others at least right magnitude	good: - some binding energies reproduced very accurately, others at least right magnitude	bad: - mostly far too repulsive due to overly strong Cr-Cr repulsion
dumbbell orientation	good: - <111>-<110> energy	good: - <111>-<110> energy	bad: - fails to reproduce all

energy differences with different occupations	difference trend reproduced bad: - fails to reproduce trends involving <100> dumbbells (though this is less relevant)	difference trend reproduced bad: - fails to reproduce trends involving <100> dumbbells (though this is less relevant)	trends
long-range repulsion from background Cr	good: - either quite accurate or at least right magnitude	good: - either quite accurate or at least right magnitude	bad: - too weak, wrong sign
background Cr does not on average bias binding of Cr to interstitials	good: - no average bias in binding strength	good: - no average bias in binding strength	good: - no average bias in binding strength
di- and tri-interstitials			
stability of ring cluster	bad: - 17 out of 32 transformed	bad: - 17 out of 32 transformed	good: - only 4 out of 32 transformed
some bindings to parallel <110> clusters can be extrapolated from binding to a single <110> interstitial	good: - irrelevance of neighbouring FeFe <110> dumbbells reproduced	good: - irrelevance of neighbouring FeFe <110> dumbbells reproduced	good: - irrelevance of neighbouring FeFe <110> dumbbells reproduced
long-range repulsion from Cr background	good: - average repulsion same order of magnitude as DFT	good: - average repulsion same order of magnitude as DFT	bad: - is essentially underestimated
background Cr does not on average bias binding of Cr to clusters	good: - no average bias in binding strength	good: - no average bias in binding strength	good: - no average bias in binding strength

5 Discussion and conclusions

FeCr is a challenging alloy to model using a semi-empirical approach. Many properties are directly linked to magnetic effects, for the bulk alloy as well as for defect – solute interactions and magnetism is to date not explicitly included in any alloy potential. The two potentials previously available in the literature (2BMpot and CDMpot) were fitted to slightly different data sets. Both attempted to reproduce the complex h.o.f. of the alloy (below the Curie temperature). The CDMpot did this almost perfectly but did not take

into account defects at all in the fitting. The 2BMpot has the caveat of a symmetric h.o.f. but does remarkably well reproduce defect – solute interactions beyond its fitting range. The motivation behind the Bon2BM was to improve on the 2BMpot in the area of defect free structures and thermodynamics. This has been achieved, considering the elimination of the stable equimolar structure predicted by the 2BMpot and by correctly reproducing the asymmetric enthalpy of mixing.

The strong and long ranged Cr – Cr repulsion is not absolutely coherent with DFT for any of the three potentials, but they all exhibit qualitative agreement. The CDMpot is too short ranged and too strong; the 2BMpot and Bon2BMpot are too weak but with the correct range. The implications for the clustering of solute Cr atoms as a first step toward precipitation as predicted by these models, would be that the critical size for nucleation should be bigger with the CDMpot and smaller with the 2BMpot and Bon2BMpot, as compared to what a kinetic model directly using DFT input would provide.

The self-interstitial – solute Cr interactions predicted by 2BMpot and Bon2BMpot are overall in better agreement with DFT than CDMpot is, which is not surprising since the <110>–FeCr mixed dumbbell was included in the fitting for the 2BMpot and Bon2BMpot but no defect configuration was considered in the fitting of the CDMpot. Thus, for studies of defect evolution and interaction the 2BM based potentials are certainly the more pertinent choice. To distinguish between them for defect interactions is difficult. Their interstitial interaction properties are mostly identical.

Using a flexible enough formalism one can of course fit anything, but for these semi-empirical potentials it is seen that many properties not fitted, or even considered during the fitting process can be reliably reproduced, with respect to DFT. Certainly, many properties are far from being reproduced but most of those are somewhat esoteric, such as the <100> self-interstitial configurations. Overall, the most convincing alloy potential for FeCr is the Bon2BMpot, due to its improvements upon the 2BMpot for defect free structures, while retaining the well reproduced defect interactions.

References
1   M. Victoria, S.L. Dudarev, J.L. Boutard, E. Diegele *et al*., Fusion Eng. Desig. **82** (2007) 2413.
2   L. Malerba, A. Caro, J. Wallenius, J. Nucl. Mater. **382** (2008) 112.
3   S.L. Dudarev, J.-L. Boutard, R. Laesser, M.J. Caturla, P.M. Derlet, M. Fivel *et al*., J. Nucl. Mater. **386** (2009) 1.
4   A. Hishinuma, A. Kohyama, R. L. Klueh, D. S. Gelles, W. Dietz and K. Ehrlich, J. Nucl. Mater. **258-263**, (1998) 193.
5   F. A. Garner, M. B. Toloczko and B. H. Sencer, J. Nucl. Mater. **276** (2000) 123.
6   P. Olsson, I. A. Abrikosov, L. Vitos and J. Wallenius, J. Nucl. Mater. **321** (2003) 84.
7   P. Olsson, I. A. Abrikosov and J. Wallenius, Phys. Rev. B **73** (2006) 104416.
8   A. A. Mirzoev, M. M. Yalalov and D. A. Mirzaev, Phys. Met. Metallogr. **97** (2004) 336.
9   T. P. C. Klaver, R. Drautz and M. W. Finnis, Phys. Rev. B **74** (2006) 094435.
10   I. Mirebeau, M. Hennion and G. Parette, Phys. Rev. Lett. **53** (1984) 678.
11   V. V. Sagaradze, I. I. Kositsyna, V. L. Arbuzov, V. A. Shabashov and Y. I. Filippov, Phys. Met. Metallogr. **92** (2001) 505.
12   G. Bonny, D. Terentyev and L. Malerba, Scr. Mater. **59** (2008) 1193.
13   Andersson, B. Sundman, CALPHAD **11** (1987) 83.
14   A. Caro, D. A. Crowson and M. Caro, Phys. Rev. Let. **95** (2005) 075702.
15   P. Olsson, J. Wallenius, C. Domain, K. Nordlund and L. Malerba, Phys. Rev. B **72** (2005) 214119.
16   P. Olsson, J. Wallenius, C. Domain, K. Nordlund and L. Malerba, Phys. Rev. B **74** (2006) 229906(E).
17   T.P.C. Klaver, P. Olsson and M.W. Finnis, Phys. Rev. B **76** (2007) 214110.
18   P. E. Blöchl, Phys. Rev. B **50** (1994) 17953.

19   G. Kresse and D. Joubert, Phys. Rev. B **59** (1999) 1758.
20   23G. Kresse and J. Hafner, Phys. Rev. B **47** (1993) RC558.
21   24G. Kresse and J. Furthmuller, Phys. Rev. B **54** (1996) 11169.
22   C. Dimitrov, A. Benkaddour, C. Corbel and P. Moser, Ann. Chim. Fr. **16** (1991) 319.
23   O. Redlich and A.T. Kister, Indust. Eng. Chem. **40** (1948) 345.
24   N. Saunders and A.P. Miodownik, *CALPHAD (Calculation of Phase Diagrams): A Comprehensive Guide*, Pergamon, Oxford, 1998.
25   G.J. Ackland and S.K. Reed, Phys. Rev. B **67** (2003) 174108.
26   G. Bonny, R.C. Pasianot and L. Malerba, Philos. Mag. **89** (2009) 711.
27   C. Pareige, C. Domain, P. Olsson, J. Appl. Phys. **106** (2009) 104906.
28   D. Terentyev, T.P.C. Klaver, P. Olsson, M.-C. Marinica, F. Willaime, C. Domain and L. Malerba, Phys. Rev. Lett. **100** (2008) 145503.
29   F. Gao, D. J. Bacon, Yu.N. Osetsky, P. E. J. Flewitt and T. A. Lewis, J. Nucl. Mater. **276** (2000) 213.
30   F. Maury, P. Lucasson, A. Lucasson, F. Faudot, J. Bigot, J. Phys. F: Met. Phys. **17** (1987) 1143
31   H. Abe and E. Kuramoto, J. Nucl. Mater. **271&272** (1999) 209-213.
32   P. Olsson, C. Domain and J. Wallenius, Phys. Rev. B **75** (2007) 014110.
33   A. Benkaddour, C. Dimitrov and O. Dimitrov, Mat. Sci. Forum **15-18** (1987) 1263.
34   C. Dimitrov, A. Benkaddour, C. Corbel, P. Moser, Ann. Chim. Fr. **16** (1991) 319.
35   A.L. Nikolaev, J. Phys.: Condens. Matter. **11** (1999) 8633-8644.
36   P. Erhart, B. Sadigh, A. Caro, Appl. Phys. Lett. 92 (2008) 141904.
37   A. Caro, M. Caro, P. Klaver, B. Sadigh, E. M. Lopasso, and S. G. Srinivasan, JOM **59** (2007) 52-57.
38   P. Erhart, A. Caro, M. Serrano de Caro and B. Sadigh, Phys. Rev. B **77** (2008) 134206.
39   G. Bonny, D. Terentyev and L. Malerba, Comp. Mater. Sc. **42** (2008) 107.
40   G. Bonny, D. Terentyev and L. Malerba, Phys. Rev. B **79** (2009) 104207.
41   P. Olsson, J. Nuc. Mat. **386–388** (2009) 86.